THE ASTROPHYSICAL JOURNAL, 402:635–642, 1993 January 10

GRAVITATIONAL FORMATION TIMES AND STELLAR MASS DISTRIBUTIONS FOR STARS OF MASS 0.3–30 $M_\odot$

P. C. MYERS AND G. A. FULLER
Harvard-Smithsonian Center for Astrophysics, 60 Garden Street, Cambridge, MA 02138
Received 1992 April 27; accepted 1992 July 15

ABSTRACT

The width of the 1.3 cm line of NH_3 in a dense core is related by simple power laws to the luminosity and mass of the most massive star associated with the core. These relations link the mass of the star to the initial conditions in the gas which formed the star. At the size scale ~ 0.1 pc of NH_3 line observations, the effects of stellar winds on the core velocity dispersion are estimated from observations of cores with and without stars, and from the dependence of the wind momentum flux on stellar luminosity. The estimated wind contribution increases with stellar luminosity, but is generally comparable to or less than the nonstellar contribution to the nonthermal motions, which is probably of magnetic origin. The wind contribution is removed from the observed velocity dispersion to estimate the velocity dispersion in the prestellar core gas. This dispersion is used to estimate the time for a core associated with a star of mass 0.3–30 $M_\odot$ to form such a star. The infall model includes both thermal and nonthermal motions. The nonthermal part of the velocity dispersion in the region which contains one stellar mass of gas is assumed to be bounded by values (*a*) the same as observed at the radius r_{obs}, and (*b*) smaller than observed by a factor $(r/r_{obs})^{1/2}$. The predicted infall times for stars of mass 0.3, 3, and 30 $M_\odot$ are 1–2, 4–8, and 1–12 $\times 10^5$ yr. The range of gravitational formation times is at most a factor of 10, significantly smaller than the factor of 100 in the range of stellar masses. A cloud forming a star cluster can produce a distribution of stellar masses which matches that of the IMF for stars more massive than 2–3 $M_\odot$, provided cores have pressure proportional to that of the underlying cluster cloud, and velocity dispersion related to stellar mass as indicated by NH_3 line observations.

Subject headings: ISM: clouds — ISM: molecules — stars: formation — stars: luminosity function, mass function

1. INTRODUCTION

A better understanding of star formation and early stellar evolution requires knowledge of the time scales, spatial scales, and energetics of the main processes at work. In the last decade, much progress has been made in understanding low-mass star formation (e.g., Shu, Adams, & Lizano 1987). Isolated stars with mass less than about 1 $M_\odot$ have parent "dense cores" whose thermal motions dominate their nonthermal motions, according to observations of the 1 cm lines of NH_3 in nearby dark clouds (Myers & Benson 1983; Benson & Myers 1989, hereafter BM; Myers, Ladd, & Fuller 1991, hereafter MLF). These observations indicate that many low-mass dense cores can be described as regions of a few solar masses of gas, supported against gravity by primarily thermal motions at a kinetic temperature of 10 K. These aspects of low-mass cores match the properties of the isothermal sphere, whose mass infall rate during "inside-out" gravitational collapse is approximately σ^3/G, where σ is the sound speed and G is the gravitational constant (Shu 1977). For these regions, the duration of the infall which produces a star of mass M_* is $M_* G/\sigma^3$. Thus it takes 6×10^5 yr for a thermal core at 10 K to accrete 1 $M_\odot$ of gas into a star, or star-disk system.

Understanding the formation of more massive stars has four additional difficulties: (1) the lack of a clear link between the properties of the parent cores and the stars they produce (e.g., Silk 1988), (2) the dominance of poorly understood nonthermal motions over thermal motions, (3) uncertainty as to the relative importance of winds, and other nonthermal motions in the observed velocity dispersion, and (4) the tendency of massive stars to appear in clusters, suggesting that the formation of massive stars involves interaction with their cluster neighbors (e.g., Larson 1990).

In this paper we address these four points. Section 2 presents empirical relations between the luminosity and mass of a star and the NH_3 line width of the associated core. Section 3 estimates the contribution of stellar winds to the observed velocity dispersion in a core with an associated star, to obtain a more accurate estimate of the mass accretion rate in the core before the star formed. Section 4 presents estimates of the star formation time for three relations between the observed line widths and the nonthermal velocity dispersion in the region of the core which collapses to form the star. Section 5 compares the distribution of stellar mass in a cluster-forming cloud with that of the IMF, based on the empirical relations between stellar mass and core velocity dispersion, and on a simple model of the cloud pressure distribution.

2. RELATION OF CORE LINE WIDTH TO STELLAR LUMINOSITY AND MASS

MLF combined the data of Wouterlout, Walmsley, & Henkel (1988, hereafter WWH) for cores associated with massive stars, and of BM for cores associated with low-mass stars, to express the typical thermal and nonthermal parts of the velocity dispersion in a core in terms of the luminosity L_* of the associated *IRAS* source. The same data can also be summarized in terms of Δv_{obs}, the FWHM of the observed NH_3 line, corrected for hyperfine, optical depth, and instru-

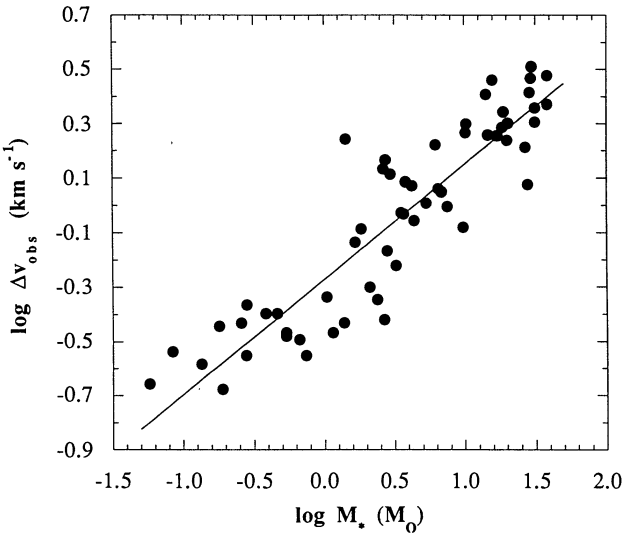

FIG. 1.—Log-log plot of the FWHM Δv_{obs} of the 1.3 cm $(J, K) = (1, 1)$ line of NH_3 in a dense core vs. the mass of the most massive associated star, based on its *IRAS* luminosity and on relations beween the mass and luminosity of young stars. The solid line is the least-squares linear fit, given in eq. (2).

mental broadening, and L_*. The best linear fit between log Δv_{obs} and log L_*, for $-1.3 < \log L_* < 5.6$, with L_* in solar units, is

$$\log \Delta v_{obs} = (-0.43 \pm 0.02) + (0.17 \pm 0.01) \log L_* , \quad (1)$$

where Δv_{obs} is in km s^{-1} and the best-fit parameters are given with their 1 σ uncertainties. WWH presented a similar relation (their eq. [1]) for their data. Myers & Fuller (1992, hereafter MF) presented a relation in their equation (21) between L_* and M_*, combining the main-sequence relation $L_* \sim M_*^{3.3}$ for more massive stars with a relation based on the "birthline" for young, low-mass stars presented by Stahler (1983). Figure 1 shows the NH_3 line data compiled by MLF, with the stellar luminosities replaced by stellar mass according to MF equation (21). The core line widths and associated stellar masses are clearly correlated. The best-fit linear relation between log Δv_{obs} and log M_* is, for $-1.3 < \log M_* < 1.6$,

$$\log \Delta v_{obs} = (-0.26 \pm 0.02) + (0.42 \pm 0.03) \log M_* . \quad (2)$$

The dependence of line width on stellar mass is much greater than the dependence of temperature on stellar mass (not shown). The more massive stars in the observed sample are probably accompanied by lower mass cluster members in many cases. If so, the mass given in equation (2) is the stellar mass responsible for most of the observed *IRAS* luminosity, i.e., the mass of the most luminous embedded cluster member.

3. VELOCITY DISPERSION IN THE PRESTELLAR CORE

The interaction of stellar winds and outflows with the circumstellar gas in the core increases the velocity dispersion over its value prior to the onset of the wind, and probably also over its value prior to the formation of the star. We estimate the increase, in order to determine the probable prestellar velocity dispersion in a core associated with a star. The observed FWHM velocity width Δv_{obs} of a line from a molecule of mass m_{obs} is related to the velocity dispersion σ of the molecule of mean mass m, and to the components of σ by

$$\Delta v_{obs}^2 = 8 \ln 2[(m/m_{obs})\sigma_T^2 + \sigma_{NT}^2 + \sigma_W^2] \quad (3)$$

and

$$\sigma^2 = \sigma_T^2 + \sigma_{NT}^2 + \sigma_W^2 \equiv \sigma_{TNT}^2 + \sigma_W^2 , \quad (4)$$

where the subscripts represent contributions due to thermal motions (T), nonthermal motions of nonstellar origin (NT), the quadrature sum of thermal motions and nonthermal motions of nonstellar origin (TNT), and winds (W). For observations of NH_3, $m/m_{obs} = 2.33/17 = 0.137$. The estimated velocity dispersion in the prestellar core is then σ_{TNT}, the velocity dispersion whose wind contribution has been subtracted in quadrature.

Eight of the cores observed by BM have associated stars with L_* within a factor of 2 of 1 $L_\odot$, and 12 otherwise similar cores have no associated stars. The FHWM line widths for these two groups have mean $\pm$ standard error of the mean 0.34 ± 0.02 km s^{-1} for the cores with stars and 0.27 ± 0.01 km s^{-1} for the cores without stars. The quadrature difference in the mean line widths is then 0.21 ± 0.03 km s^{-1}. For a probable upper bound on the effects of winds from stars with 1 $L_\odot$ we attribute all of this difference to winds. We denote the corresponding velocity dispersion, 0.088 km s^{-1}, as $\sigma_{W,1}$.

In regions of more massive star formation, several "starless" cores are known. NH_3 line maps whose position of maximum emission is 1.3 to 2.9 FWHM map diameters from the nearest star with $L_* > 10^3$ $L_\odot$ include cores north of HD 200775 ($L_* = 4 \times 10^3$ $L_\odot$; Fuente et al. 1990; Chokshi et al. 1988); west of S106 (1×10^4 $L_\odot$; Stutzki, Ungerechts, & Winnewisser 1982; Barsony et al. 1989); east of GGD 12−15 (8×10^3 $L_\odot$; Güsten & Marcaide 1986; Harvey et al. 1985); north of NGC 2264 (3.5×10^3 $L_\odot$; Harvey, Campbell, & Hoffman 1977); and north of S140 (1×10^4 $L_\odot$; Tafalla, Bachiller, & Martín-Pintado 1993; Evans et al. 1989). These have line widths $\Delta v_{obs} = 0.5$ to 1.6 km s^{-1} and kinetic temperatures 14 to 20 K. They are dominated by nonthermal motions in all but the HD 200775 core, where the thermal and nonthermal motions are essentially equal. Thus these massive starless cores are generally nonthermal, unlike the low-mass cores. The nonthermal line widths in these massive cores are unlikely to arise from stellar winds, since the associated stars are too far from the cores (MLF). However, these cores are too few in number to allow a reliable statistical estimate of the effects of winds on core line widths, as was done above the low-mass cores. Consequently we extend the model of MLF describing the interaction of a stellar wind with its surrounding dense gas, with two new aspects: the virial support of the core and dependence of the rate of production of stellar wind momentum on stellar luminosity.

The basic physical picture is that of a star, or star-disk system, at the center of a dense core. The core is spherically symmetric, except for a biconical outflow channel, which contains gas of lower density than in the core, moving outward in excess of the escape speed, as revealed by the wings of the CO line. The interaction of the winds and outflow gas with the core gas near the boundary of the outflow channel generates turbulent motions in the core gas.

Based on the correlations in MLF,

$$\sigma_{NT}^2 + \sigma_W^2 \equiv \sigma_{NTW}^2 = c_{NTW} l^{0.38} \quad (5a)$$

$$\sigma_T^2 = c_T l^{0.082} , \quad (5b)$$

where equation (5a) defines σ_{NTW}, where $c_{NTW} = 0.018$ km^2 s^{-2}, $c_T = 0.038$ km^2 s^{-2}, and $l \equiv L_*/L_\odot$ is the bolometric stellar luminosity in solar units. The rate of production of stellar wind momentum due to winds, dP_+/dt, can be written

$(dM/dt)v_w$, where dM/dt is the mass-loss rate and v_w is the wind speed. In a study of CO outflows from 23 optically selected young stars with $0.7 \leq \log l \leq 5.1$, Levreault (1988) found that $\log dM/dt = (-7.8 \pm 0.3) + (0.6 \pm 0.1) \log l$, where dM/dt is in $M_\odot$ yr^{-1}. Following Levreault, we adopt $v_W = 300$ km s^{-1}, so that

$$dP_+/dt = el^{0.6} , \quad (6)$$

where $e = 4.8 \times 10^{-6} M_\odot$ km s^{-1} yr^{-1}.

The rate of loss of momentum into turbulent motions in the core gas traced by the NH_3 lines can be written

$$dP_-/dt = \alpha M_{obs} \sigma_W / (r_{obs}/\sigma_W) , \quad (7)$$

where M_{obs} and r_{obs} are the core mass and radius traced by the NH_3 lines, r_{obs}/σ_W is the approximate rotation period of the largest turbulent eddies within r_{obs}, and α is a dimensionless constant of order unity. Equation (7) assumes that the largest eddies within r_{obs} have dimension r_{obs}, and that their dissipation time is equal to their rotation period. We assume that the core is in approximate virial equilibrium, as is usually observed (Myers et al. 1991), and that the effect of the winds is to increase the core pressure over its prestellar value. then $M_{obs}/r_{obs} = \beta\sigma^2/G$, where β is a dimensionless constant depending on the density profile in the core, and

$$dP_-/dt = \alpha\beta\sigma_W^2/G . \quad (8)$$

We assume a steady state condition where a fraction γ of the wind momentum production rate is coupled into turbulent motions of the core gas, $\gamma(dP_+/dt) = dP_-/dt$, and where γ is independent of the stellar luminosity l. Then from equations (6) and (8),

$$\gamma = \frac{\alpha\beta\sigma^2\sigma_W^2}{Gel^{0.6}} = \frac{\alpha\beta(c_T + c_{NTW})\sigma_{W,1}^2}{Ge} \quad (9)$$

where the right-hand expression in equation (9) is evaluated for $l = 1$ and $\sigma_W = \sigma_{W,1}$, as discussed above. For a core in virial equilibrium, $\beta = 9/2$ when the density profile is $n \sim r^{-1}$ and $\beta = 3$ when $n \sim r^{-2}$. Then for $\alpha = 0.5 - 2$, equation (9) indicates that the momentum rate coupling constant $\gamma = 3\%$–18%.

Equations (6), (8), and (9) give the wind contribution to the core velocity dispersion in terms of the stellar luminosity.

$$\sigma_W = \sigma_{W,1}\left[\frac{1 + c_T/c_{NTW}}{l^{-0.22} + (c_T/c_{NTW})l^{-0.52}}\right]^{1/2} \quad (10)$$

or

$$\sigma_W = 0.15(l^{-0.22} + 2.1l^{-0.52})^{-1/2} \text{ km s}^{-1} . \quad (11)$$

Since equations (10) and (11) for σ_W are "normalized" to $\sigma_{W,1}$, they are independent of the relatively uncertain parameters α, β, γ, and e.

Equation (11) indicates that the wind contribution to the total velocity dispersion ranges from 0.07 km s^{-1} when $l = 0.3$, to 0.5 km s^{-1} when $l = 1 \times 10^5$. This contribution is smaller by a factor of 1.2 to 2.0 than the nonthermal σ_{NT} for all l, indicating that the wind contribution is significant, but not dominant, for core support. An alternative model, in which a constant fraction of the wind kinetic energy production rate is coupled into turbulent motions, gives smaller values of σ_W than in equations (10) and (11): in equation (10) the exponent $\frac{1}{2}$ is replaced by $\frac{1}{3}$, and the maximum value of σ_W becomes 0.3 rather than 0.5 km s^{-1}.

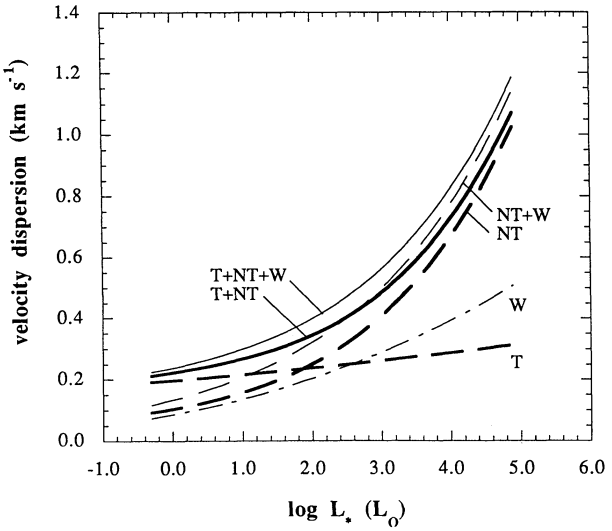

FIG. 2.—Velocity dispersions in a dense core associated with a star of luminosity L_*, on the size scale ~ 0.1 pc sampled by NH_3 observations. The curves are based on empirical relations between line width and luminosity, kinetic temperature and luminosity, stellar wind momentum flux and luminosity, and on a model of turbulent broadening of the core gas by winds. Curves marked T, W, and NT show contributions to the velocity dispersion due to thermal heating, winds, and large-scale nonthermal motions. Curves marked NT + W, T + NT, and T + NT + W show quadrature sums of the individual contributions. Heavy curves T, NT, and T + NT show the velocity dispersions used to describe the conditions in the prestellar core.

Figure 2 shows the dependence of the velocity dispersion in the NH_3 core on the log of the associated stellar luminosity, for six dispersions. Four are computed from equations given above: σ_W from equation (11), σ_T from equation (5b), σ_{NTW} from equation (5a) and σ from equation (4). Figure 2 also shows two dispersions with the wind contribution removed: $\sigma_{TNT} = (\sigma^2 - \sigma_W^2)^{1/2}$, and $\sigma_{NT} = (\sigma_{NTW}^2 - \sigma_W^2)^{1/2}$. These two and the thermal dispersion σ_T are shown in heavy lines, since they are used for the infall calculations in § 4. All six of the dispersions increase with increasing stellar luminosity.

Figure 2 indicates that the wind contribution σ_W to the total velocity dispersion exceeds the thermal contribution σ_T for $l > 400$, but in no case does the broadening due to winds dominate the total dispersion: at low luminosity the wind contribution is significantly less than the thermal contribution, and at high luminosity the wind contribution is significantly less than the nonthermal contribution σ_{NT}. The ratio of the nonthermal velocity dispersion, corrected for winds, σ_{NT}, to that uncorrected for winds, σ_{NTW}, is 0.8–0.9 over the range of stellar luminosities considered here.

The uncertainty in the model predictions can be crudely judged by comparing with data from the five "starless" cores in regions of massive star formation, cited earlier in this section. In the median case, the model underestimates σ_{NTW} by 10%, overestimates σ_{NT} by 50%, underestimates σ_W by 30%, and overestimates σ_{NT}/σ_{NTW} by 25%. These uncertainties do not change the main conclusions of this paper. It will be valuable to obtain more data on starless cores, to correct and refine the estimates presented here. A related discussion of eight starless cores in Orion is given by Myers & Fuller (1993).

The relative contribution of winds to the velocity dispersion should depend strongly on the size and density scale over which the observed tracer line is sensitive. A line which traces smaller circumstellar size scales than does the NH_3 line should reveal a greater influence from stellar winds than is evident here, when comparison is made between cores with and without stars. On such small scales, winds and outflows probably increase the pressure in the core enough to halt the infall. At larger sizes and lower densities, such as those traced by the $J = 1$–0 line of ^{13}CO, the relative wind contribution should be smaller than found here. For example, observations of 51 cores in northern Ophiuchus in the 1–0 line of ^{13}CO found eight cores with associated *IRAS* sources and/or T Tauri stars and 43 cores with no associated star (Nozawa et al. 1991). The line widths in these two groups have mean $\pm$ standard error of the mean 1.05 ± 0.12 km s^{-1} and 0.96 ± 0.04 km s^{-1}. The quadrature difference, calculated in the same manner as for the NH_3 line data above, is 0.4 ± 0.3 km s^{-1}, which is statistically indistinguishable from zero.

4. STAR FORMATION TIMES

The time t_{acc} from the onset of spherical collapse to accrete a particular mass M_* depends on the radial profile of the gas density within the radius r_{col}, which encloses M_*. In a self-gravitating equilibrium model, the density profile within r_{col} is related to the radial profile of the velocity disperson within r_{col}. The calculations of t_{acc} presented here are based on differing inferences from the observed data about the velocity dispersion within r_{col}.

To calculate t_{acc} we use equation (1) and MLF equations (3) and (4) to infer the thermal and nonthermal components of the velocity dispersion in a core of radius r_{obs}, traced by the NH_3 lines, which is typically associated with a star of mass M_*. The nonthermal component of the velocity dispersion is corrected for the effects of winds from the associated star as in § 3 above. We assume that the resulting σ_{NT} describes the nonthermal motions at r_{obs} in the prestellar core, and that σ_T describes to sufficient accuracy the thermal motions at all r in the prestellar core, which is assumed isothermal. No correction is made here for stellar heating of core gas, because according to Figure 2 even the hottest core temperatures provide a negligible contribution to the total velocity dispersion. Also, no correction is made here for the effects of winds from the protostar, in modifying and eventually terminating the infall: the termination is crudely assumed to be "sudden." We relate $\sigma_{NT}(r \leq r_{col})$ to $\sigma_{NT}(r_{obs})$ according to the following possible cases.

1. $\sigma_{NT}(r \leq r_{col}) = \sigma_{NT}(r_{obs})$, i.e., the observed value of the nonthermal velocity dispersion, corrected for winds, is uniform for all $r \leq r_{obs}$.

2. $\sigma_{NT}(r \leq r_{col}) = (r/r_{obs})^{1/2}\sigma_{NT}(r_{obs})$, i.e., the nonthermal velocity dispersion is smaller than at r_{obs} according to the relation $\sigma_{NT} \sim r^{1/2}$ characteristic of some star-forming regions. This case differs from that calculated by MF, in that here the observed nonthermal velocity dispersion is corrected for winds.

3. $\sigma_{NT}(r \leq r_{col}) = 0$, i.e., the nonthermal motions are negligible, and the accretion time depends only on the thermal motions. This case is identical to that presented by MF.

We consider cases (1) and (2) to bracket the likely range of possibilities, and present the thermal case (3) for comparison. These cases are illustrated schematically in Figure 3.

For cases (1) and (3) $\sigma_{NT}(r \leq r_{col})$ is uniform, so the accretion time is calculated as in the isothermal case, except that in case

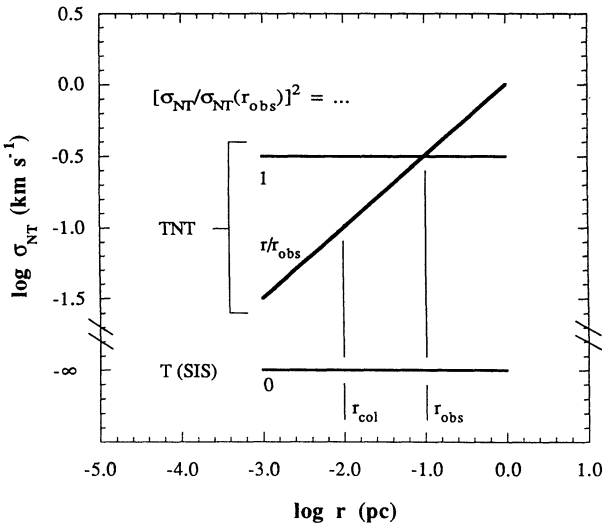

FIG. 3.—Schematic diagram illustrating three assumptions about the radial structure of the nonthermal part of the velocity dispersion σ_{NT} in a prestellar core. The horizontal curve marked $[\sigma_{NT}/\sigma_{NT}(r_{obs})]^2 = 1$ indicates that the inside radius r_{col} which encloses one stellar mass, the nonthermal velocity disperson is the same as at the size scale r_{obs} sampled by NH_3 observations. The sloping curve marked r/r_{obs} indicates that the nonthermal velocity dispersion is smaller than observed by a factor $(r/r_{obs})^{1/2}$. These two cases, marked TNT, take into account both the thermal and the nonthermal motions observed in line widths and are considered to bracket the likely range of possibilities. The horizontal curve marked $[\sigma_{NT}/\sigma_{NT}(r_{obs})]^2 = 0$ and T(SIS) indicates that the nonthermal motions are neglected, and that the remaining thermal motions are assumed constant, as in the singular isothermal sphere.

(1) the thermal component is accompanied by a nonthermal component:

$$t_{acc} = M_* G[\sigma_{NT}^2(r_{col}) + \sigma_T^2]^{-3/2} . \quad (12)$$

In equation (12), the relation of σ_T to M_* is known from MLF equation (4) and from the luminosity-mass relations given in MF equation (21). In case (3), $\sigma_{NT}(r_{col}) = 0$, so no further information is needed to solve equation (12). In case (1), $\sigma_{NT}(r_{col}) = \sigma_{NT}(r_{obs})$, and $\sigma_{NT}(r_{obs})$ is related to M_* from MLF equation (3) and from MF equation (21). For case (2), the calculation of $t_{acc}(M_*)$ in MF was repeated, with the wind correction described in § 3 above, for the two assumed values of the mean density in the region of NH_3 emission, $n_{obs} = 10^3$ and 10^4 cm^{-3}. The accretion times in this case are only slightly longer than in MF.

Figure 4 shows curves of log t_{acc} vs log M_* for the three cases described above. The cases (1) and (2) which take nonthermal motions into account have shorter formation times than does the thermal case (3), since the greater velocity dispersions in cases (1) and (2) imply greater accretion rates. For these two cases, the range of formation times for stars of mass 0.3, 1, 3, 10, and 30 $M_\odot$ is 1.1–1.5, 3–4, 4–8, 2–11, and 1–12 $\times$ 10^5 yr. All of the stars considered form in 1–12 $\times$ 10^5 yr, with the greatest range for most massive stars. Therefore the range of stellar formation times is significantly smaller than the range of stellar masses formed by molecular clouds.

It is well known that the Kelvin-Helmholtz time t_{KH} for the stellar core to reach thermal equilibrium exceeds the gravitational infall time t_{acc} for sufficiently massive stars (Clayton 1968). The results presented in this paper indicate that $t_{KH} = t_{acc}$ for $M_* = 5\ M_\odot$.

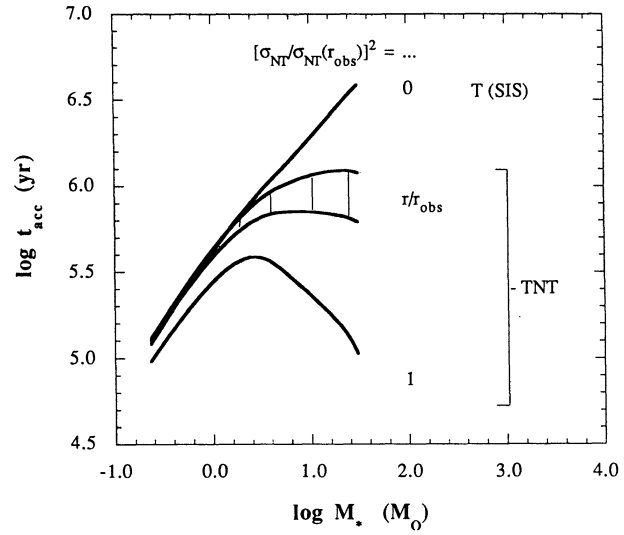

FIG. 4.—Gravitational formation times t_{acc} for a core associated with a star of mass M_* to form a star, or star-disk system, of that mass. The three cases are marked according to the assumptions about the radial structure of the nonthermal part of the velocity dispersion, illustrated in Fig. 3. The range of times in the case marked r/r_{obs} correspond to mean density in the region of NH_3 line excitation 10^3 cm^{-3} (*upper*) and 10^4 cm^{-3} (*lower*). The cases marked TNT take both thermal and nonthermal motions into account and bracket the likely range of possibilities. For them the range of star formation times is 1–12 × 10^5 yr. This range of a factor of 12 is significantly smaller than the factor of 100 in the range of stellar masses.

It will be useful to obtain systematic measurements of line width and map size in the densest parts of cores in regions of massive star formation, to better constrain the estimates presented here.

5. FORMATION OF STARS IN CLUSTERS

The estimates of gravitational star formation time presented in § 4 are for single stars, whereas most massive stars, and perhaps even most low-mass stars, are believed to form in open clusters (Larson 1990; Lada & Lada 1991). In § 5.1 we use the relations among core velocity dispersion and stellar mass, presented earlier, to estimate the distribution of stellar masses in a cluster-forming cloud. Under simple assumptions, it appears possible to match the form of the initial mass function (IMF) for stars more massive than 2–3 $M_\odot$. More limited discussions are also presented on the progression of stellar mass formed over the life of the cluster cloud, in § 5.2, and on the role of stellar winds in providing increased support for cores in the central part of the cluster cloud, in § 5.3.

5.1. *Distribution of Stellar Masses in a Cluster Cloud*

The cluster-forming cloud is assumed to consist of a spherically symmetric "cloud" component, whose velocity dispersion varies with radius R as R^{-q}. The cloud is self-gravitating, so that its density varies as R^{-2+2q}, and its pressure varies as R^{-2+4q}. Smaller, spherical self-gravitating "cores" are embedded in the cloud and have total mass small compared to the cloud mass. In the star-forming part of a core, the pressure and density are much greater than corresponding pressure and density contributed by the cloud component. At the core radius r_{obs} traced by NH_3 observations, the pressure $P(r_{obs})$ is assumed to be a fixed multiple g of the pressure of the cloud component. The variation in cloud pressure across r_{obs} is assumed negligibly small compared to the mean core pressure within r_{obs}. Cores with high pressure have greater velocity dispersion within r_{obs} than do cores with low pressure, and therefore tend to form more massive stars, according to the relations in § 2. Thus the model cluster-forming cloud has a high-pressure interior, with high-pressure cores, making more massive stars, and a low-pressure exterior, with low-pressure cores, making less massive stars. Stars in a given range of stellar mass tend to form within a particular range of cloud radius and pressure. The tendency for more massive stars to be concentrated toward the centers of young clusters was discussed by Larson (1982).

The distribution of stellar masses produced in this model is estimated by computing $\xi \equiv dN/d\log M_*$, the number of stars per logarithmic mass interval around M_*. We define $M(M_*) \equiv NM_*$ as the total mass in stars with mass in a fixed interval ΔM around M_*, $M_{cloud}(M_*)$ as the total cloud mass associated with stars of mass in the interval ΔM around M_*, and $\epsilon(M_*) \equiv M(M_*)/M_{cloud}(M_*)$. We assume that $\epsilon(M_*)$ is independent of M_*, i.e., the star formation efficiency $S = \epsilon/(1+\epsilon)$ in the cluster is independent of stellar mass. The mass of cloud gas within radius R is $M(<R) \sim R^{1+2q}$, so the mass of cloud gas above a given pressure P_{cloud} is $M(>P_{cloud}) = h(P_{cloud})^y$, where h is a constant and $y \equiv (1+2q)/(-2+4q)$. Then

$$\xi = \frac{dM(M_*)}{dM_*} = \epsilon \frac{dM_{cloud}(>P_{cloud})}{dP_{cloud}} \frac{dP_{cloud}}{dP_{core}} \frac{dP_{core}}{dM_*} . \quad (13)$$

Evaluating each term on the right-hand side of equation (13) gives

$$\xi = \epsilon h y g^{-y} \rho^y \sigma^{2y} \left(\frac{1}{\rho} \frac{d\rho}{dM_*} + \frac{2}{\sigma} \frac{d\sigma}{dM_*} \right), \quad (14)$$

where the mass density ρ and the velocity dispersion σ refer to the core properties on the size scale traced by the NH_3 line. We write $C \equiv \log(\epsilon h y g^{-y})$ to group quantities independent of M_*, so that

$$\log \xi = C + \frac{1+2q}{-2+4q} (\log \rho + 2 \log \sigma) + \log \left(\frac{1}{\rho} \frac{d\rho}{dM_*} + \frac{2}{\sigma} \frac{d\sigma}{dM_*} \right) \quad (15)$$

The parts of equation (15) which depend on σ in terms of the mass M_* of the associated star are evaluated from equation (5) and from MF equation (21). The parts which depend on ρ are evaluated in two ways because the beam-averaged mass density $\rho = mn$ traced by the NH_3 lines observed by BM and WWH is uncertain, due to subbeam clumping.

Cores observed by BM associated with stars of 1 $M_\odot$ have median distance 140 pc. At this distance the diameter of the beam used by BM is 0.07 pc. In contrast the median distance of a core associated with a 30 $M_\odot$ star observed by WWH is 2 kpc, and at this distance the diameter of the beam used by WWH is 0.7 pc, larger by a factor 10 than that used by BM for cores associated with $M_* = 1\ M_\odot$. Also, low-mass cores probably have less clumpy structure than do massive cores, because low-mass cores are more dominated by thermal motions, which can easily smooth out pressure fluctuations. Thus, low-

mass cores should have a greater volume filling factor than massive cores, and the mean density in a low-mass core should be closer to that based on excitation requirements in uniform density gas. Excitation of the NH_3 (1, 1) line requires mean density $n \approx 1 \times 10^4$ cm^{-3}, which for low-mass cores is consistent with NH_3 line map sizes and estimates of visual extinction. For more massive cores, n should probably be nearer to 1×10^3 cm^{-3}, since MF found that data from the NH_3 line and from other lines agree better if $n \approx 1 \times 10^3$ cm^{-3} than if 1×10^4 cm^{-3}.

Thus to evaluate equation (14) we use two alternate forms of $\rho(M_*)$:

$$\rho/m = 3 \times 10^3 \text{ cm}^{-3} , \tag{16a}$$

which is independent of M_*, and

$$\rho'/m = 1 \times 10^4 \text{ cm}^{-3}\{[1 + (M_*/3\ M_\odot)^2]^{-1/2} + 0.05\} . \tag{16b}$$

This function ρ'/m is nearly constant at 1×10^4 cm^{-3} for $M_* \leq 1\ M_\odot$ and makes a smooth transition to 1.5×10^3 cm^{-3} at $M_* = 30\ M_\odot$. For each of these two density profiles, ξ depends on only one free parameter, the exponent q in the power-law relation between velocity dispersion and radius in the cluster cloud.

With reference to the collapse calculations in § 4, we emphasize that the densities discussed here refer to size scales $r_{obs} \gg r_{col}$. The corresponding densities at r_{col} are much greater than at r_{obs}. For example, a typical core associated with a 30 $M_\odot$ star observed by WWH might have a FWHM extent of three beam diameters. Then its mean density of 1.5×10^3 cm^{-3} as in equation (16b), above, would correspond to a radius 1 pc. In case (1) of § 4 it would enclose 30 $M_\odot$ at $r_{col} = 0.028$ pc, where it would have density 2×10^6 cm^{-3}.

For each density profile, Figure 5 shows curves of log ξ for two values of q, chosen so that the slope of log ξ vs log M_* closely matches that of the high-mass part of the IMF. For each curve the arbitrary constant C has been adjusted to facilitate comparison of the slopes. The IMF, shown in filled circles, is taken from Scalo (1986) for the case where $\tau = \infty$, i.e., where the IMF has been constant over the life of the Galaxy (changing this assumption affects only the shape of the low-mass part of the IMF). The values of q are shown with no prime for the constant density profile, equation (16a), and with a prime for the varying density profile, equation (16b).

Figure 5 shows that for each density profile, a range of q exists which closely brackets the slope of the upper part of the IMF, for stars more massive than 2–3 $M_\odot$. For constant density, equation (16a), this range is 0.1–0.2, while for density which varies as in equation (16b), this range is 0.3–0.4. The varying density case appears more realistic, for the reasons given above. Thus a self-gravitating cluster cloud having cores which follow the observed relations between core velocity dispersion and associated stellar mass can account for the slope of the IMF for stars more massive than 2–3 $M_\odot$, provided the mean core density at the radius sampled by NH_3 lines decreases with increasing M_*, as in equation (16b), and provided the cluster cloud velocity dispersion increases with radius as R^q, with $q = 0.3$–0.4. It is noteworthy that the nearest cluster cloud, L1686 in Ophiuchus, has $q = 0.3$, as expected in this model. Determination of q for more cluster clouds will be an important test of the model.

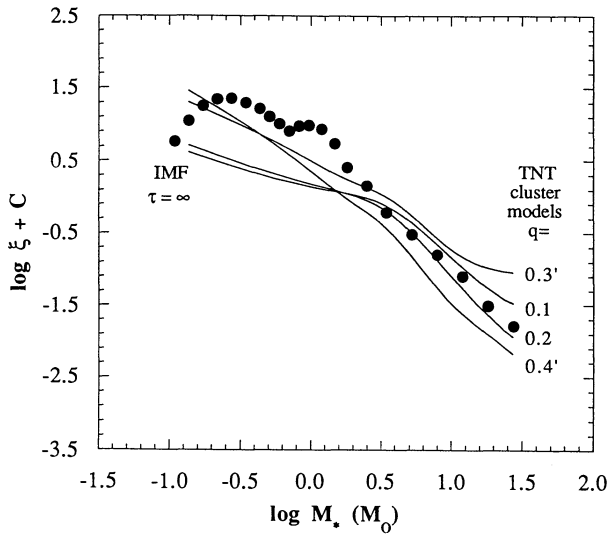

FIG. 5.—Log of the distribution of the number of stars per unit logarithmic mass interval around M_*, vs. log M_*. *Solid lines:* four models of a self-gravitating cluster cloud with embedded self-gravitating cores. Curves are labeled according to the exponent q in the power-law relation $\sigma \sim R^q$ between velocity dispersion σ and the radius R of the cluster cloud. Curves marked $q = 0.1$ and 0.2 represent embedded cores having constant mean density at the size scale traced by NH_3 line observations. Curves marked 0.3′ and 0.4′ represent cores having mean density which decreases with increasing mass of their associated star, due probably to subbeam clumping. *Filled circles:* the initial mass function (IMF) of Scalo (1986), assuming that the IMF has remained constant over the lifetime of the Galaxy.

The model is idealized because it assumes a smooth, spherical cloud geometry, but this particular geometry was chosen for convenience and is not essential. The main requirement is that the cloud gas have a distribution of pressure which allows a sufficient number of cores to form in each interval of pressure. For $q = 0.3$–0.4 as found above, the corresponding distribution of cloud mass with cloud pressure is $M_{cloud} \sim (P_{cloud})^s$, with $s = -2.0$ to -4.5. This could be met by many irregular and complex geometrical arrangements, perhaps including those seen in molecular cloud complexes. There, a characteristic distribution has a high-column density, high-pressure, slightly elongated cloud, which tends to form star clusters, and also one or several low-column density, low-pressure, filamentary clouds, which tend to form more isolated, low-mass stars (Myers 1991). A model relating hierarchical, filamentary cloud geometry to the distribution of stellar masses formed was presented by Larson (1993).

5.2. *Development of the Cluster Cloud over Time*

The foregoing picture is also idealized, in that it assumes a cluster cloud whose structure is fixed over its lifetime, typically some 5×10^6 yr (Leisawitz, Bash, & Thaddeus 1989). According to the results of § 4, the cluster cloud lifetime is of order 10 star formation times, so one may expect that of order 10 "generations" of stars can form in the cluster cloud. If so, the distribution of stellar masses can change from one generation to the next, giving a distribution over the cluster life which is the sum over its generations. In this picture, the properties of the cluster cloud discussed above would apply to a relatively evolved cloud which had already begun to produce some massive stars. It is plausible that cluster clouds evolve, for the following reasons.

Molecular cloud regions which contain embedded clusters, such as the Trapezium cluster in Orion A, NGC 2024 and NGC 2068 in Orion B, NGC 1333 in Perseus, and the HD 147889 cluster in Ophiuchus, appear denser and more massive than neighboring parts of the same clouds with less pronounced star formation (Myers 1991). The areas around embedded cluster regions tend to have greater dispersion in their directions of optical polarization than do their neighboring clouds, suggesting that gas in the cluster periphery has distorted the magnetic field lines by moving at speeds greater than the local Alfvén speed (Myers & Goodman 1991). These differences suggest that the cluster-forming parts of clouds have generally accumulated more mass than their neighboring regions, perhaps by gravitational attraction, or by accretion as clouds move through lower density gas. The process of accumulation need not have completed before the onset of star formation, and it is possible that accumulation of low-density gas at the cloud periphery is a common feature in the development of an embedded cluster.

The time scale for such accumulation is a few times 10^6 yr, if the basic process is gravitational infall of gas with density 100–300 cm^{-3}. This time is comparable to the lifetime of an embedded cluster. Such infall would double the mass of a spherical, uniform cloud of radius 3 pc and mass 2×10^3 $M_\odot$ in $1–2 \times 10^6$ yr if the infall were continuous and if it covered the surface of the cloud uniformly. In reality the doubling time would be somewhat greater, because of the more complex structure of observed clouds. This level of accumulation need not induce global collapse of the cloud, since on this scale molecular clouds appear to be relatively stable, perhaps because of the winds and radiation from newly formed stars, and because of long-wavelength hydromagnetic waves (Falgarone & Puget 1988; Pudritz 1990). Such accumulation is not excluded by observations of molecular lines, since the density is too low for all but the CO 1–0 line to reveal it, and the infall speed, 1–2 km s^{-1}, is comparable to the CO line width seen in regions of similar mass (e.g., Ungerechts & Thaddeus 1987).

If cluster clouds increase their internal pressure scale over their lifetime, their surviving cores and their newly formed cores can be expected to have greater pressure than when the cluster cloud was younger. As discussed above, increased core pressure leads to formation of more massive stars. Consequently a young, low-pressure cluster cloud should form a distribution of lower mass stars, while a more massive, high-pressure cluster cloud will tend to form a distribution with more massive stars. This sense of progression of stellar masses over time in a cluster was first discussed by Herbig (1962).

5.3. *Effects of Stellar Winds on Production of Cluster Stars*

The stars already formed in a cluster emit winds and radiation, which may inhibit or promote the formation of more massive stars by neighboring cores. If the luminous and mechanical momentum and energy coupled into a core are too great, over too short a time, they will disperse enough of the core gas to prevent formation of a star. If the coupling is weaker and more gradual, a self-gravitating core may survive with slightly increased velocity dispersion, as discussed in § 3. This increased velocity dispersion corresponds to an increased mass infall rate during collapse. The mechanisms of such an increase are not clear, mainly because the physics of the turbulent motions are poorly understood. One requirement of the coupling is that the increase in core pressure due to the effects of neighboring stars be at least as great as the increase in pressure of the core environment. Radiation from neighboring stars might meet this requirement if the core dust is optically thick, while the dust between the stars and the core is optically thin at the wavelengths of the heating radiation. A similar mechanism, involving preferential coupling of hydromagnetic wave energy into cores, has been investigated by Puget (1991).

If a low level of wind and radiation flux from external stars promotes the development of cores capable of forming more massive stars, while a high level inhibits this development, clouds may more effectively form rich clusters if they make lower mass stars in their early generations, and more massive stars in their later generations.

6. SUMMARY

The main points presented in this paper are as follows.

1. The line width Δv_{obs} of a dense core observed in the 1.3 cm lines of NH_3 is related to the luminosity and mass of the most massive star associated with the core, according to simple power laws. The line width varies approximately as L_*^p, where $q = 0.42 \pm 0.03$, for $0.3 \leq M_*/M_\odot \leq 30$.

2. The effect of stellar winds and outflows on the velocity dispersion of the core gas is estimated, assuming that a fixed fraction of the wind momentum flux is coupled into turbulent motions in the core. On the scale of the NH_3 core, the contribution by winds is significant, but smaller than the thermal motions for cores associated with low-luminosity stars and smaller than the large-scale nonthermal motions for cores associated with luminous stars. The momentum flux coupling efficiency is 3%–18%.

3. The time for a core associated with a star of mass 0.3–30 $M_\odot$ to form such a star is estimated using a model of radial gravitational infall which includes both thermal and nonthermal motions. The core velocity dispersion observed to be associated with a given stellar mass is corrected for the relatively small effects of winds, to estimate the velocity dispersion in the prestellar core at the observed size scale r_{obs}. The infall time is calculated, assuming that the velocity dispersion at the radius r_{col} which encloses one stellar mass is (*a*) equal to that at r_{obs}, or (*b*) smaller than at r_{obs} by a factor $(r_{col}/r_{obs})^{1/2}$. The infall time for stars of mass 0.3, 1, 3, 10, and 30 $M_\odot$ is 1–2, 3–4, 4–8, 2–11, and $1–12 \times 10^5$ yr. The range of formation times, at most a factor of 10, is significantly smaller than the factor of 100 in the range of stellar masses. Thus variation in the initial velocity dispersion from core to core is a key determinant of the stellar mass to be formed from that core.

4. A self-gravitating cluster-forming cloud whose velocity dispersion increases with radius as R^q, $q = 0.3–0.4$, as is observed in the L1686 cloud in Ophiuchus, can produce a distribution of stellar masses M_* similar to that of the IMF for $M_* \geq 2–3$ $M_\odot$, provided that on the size scale traced by the NH_3 lines, embedded cores have (*a*) pressure in proportion to the pressure of the underlying cluster cloud; (*b*) an increase in core velocity dispersion with increasing associated stellar mass M_*, as derived from NH_3 line observations of *IRAS* sources; and (*c*) a decrease in mean core density with increasing associated M_*, as expected for subbeam clumping in observations of distant cores associated with massive stars. This agreement with the slope of the IMF suggests that formation of stars in clusters can be understood in terms of simple physical concepts and observed core properties.

The mass and pressure of a typical cluster-forming cloud probably increase significantly over its star-forming life, requiring a corresponding increase in the pressure of the

typical embedded core, and thereby increasing the mass of the star likely to form in the core. Winds and radiation from already formed stars in the cluster may contribute to this increase in core pressure.

We thank Frank Shu and Steve Stahler for helpful discussions, and the referee, David Leisawitz, for several constructive comments. G. A. F. acknowledges the support of a Center for Astrophysics postdoctoral fellowship.

REFERENCES

Barsony, M., Scoville, N. Z., Bally, J., & Claussen, M. J. 1989, ApJ, 343, 212
Benson, P. J., & Myers, P. C. 1989, ApJS, 71, 89 (BM)
Chokshi, A., Tielens, A. G. G. M., Werner, M. W., & Castelaz, M. W. 1988, ApJ, 334, 803
Clayton, D. D. 1968, Principles of Stellar Evolution and Nucleosynthesis (NY: McGraw-Hill)
Evans, N. J., Mundy, L. G., Kutner, M. L., & DePoy, D. L. 1989, ApJ, 346, 212
Falgarone, E. D., & Puget, J.-L. 1988, in Galactic and Extragalactic Star Formation, ed. R. E. Pudritz & M. Fich (Dordrecht: Kluwer), 195
Fuente, A., Martín-Pintado, J., Cernicharo, J., & Bachiller, R. 1990, A&A, 237, 471
Güsten, R., & Marcaide, J. M. 1986, A&A, 164, 342
Harvey, P. M., Campbell, M., & Hoffman, W. 1977, ApJ, 215, 151
Harvey, P. M., Wilking, B. A., Joy, M., & Lester, D. F. 1985, ApJ, 288, 725
Herbig, G. G. 1962, Adv. Astr. Ap., 1, 47
Krügel, E., Güsten, R., Schulz, A., & Thum, C. 1987, A&A, 185, 283
Lada, C. J., & Lada, E. A. 1991, in The Formation and Evolution of Star Clusters, ed. K. Janes (San Francisco: ASP), 3
Larson, R. B. 1982, MNRAS, 200, 159
———. 1990, in Physical Processes in Fragmentation and Star Formation, ed. R. Capuzzo-Dolcetta et al. (Dordrecht: Kluwer), 389
———. 1993, MNRAS, in press
Leisawitz, D., Bash, F. N., & Thaddeus, P. 1989, ApJS, 70, 731
Levreault, R. L. 1988, ApJ, 330, 897
Myers, P. C. 1991, in Fragmentation of Molecular Clouds and Star Formation, ed. E. Falgarone et al. (Dordrecht: Kluwer), 221
Myers, P. C., & Benson, P. J. 1983, ApJ, 266, 309
Myers, P. C., & Fuller, G. A. 1992, ApJ, 396, 631 (MF)
———. 1993, in Massive Stars: Their Lives in the Interstellar Medium, ed. J. Cassinelli & E. Churchwell (San Francisco: ASP), in press
Myers, P. C., & Goodman, A. A. 1991, ApJ, 373, 509
Myers, P. C., Ladd, E. F., & Fuller, G. A. 1991, ApJ, 372, L95 (MLF)
Nozawa, S., Mizuno, A., Teshima, Y., Ogawa, H., & Fukui, Y. 1991, ApJS, 77, 647
Pudritz, R. E. 1990, ApJ, 350, 195
Puget, J.-L. 1991, talk at IAU General Assembly, Buenos Aires
Scalo, J. M. 1986, Fund. Cosmic Phys., 11, 1
Shu, F. H. 1977, ApJ, 214, 488
Shu, F. H., Adams, F. C., & Lizano, S. 1987, ARA&A, 25, 23
Silk, J. 1988, in Galactic and Extragalactic Star Formation, ed. R. E. Pudritz & M. Fich (Dordrecht: Kluwer), 503
Stahler, S. 1983, ApJ, 268, 155
Stutzki, J., Ungerechts, H., & Winnewisser, G. 1982, A&A, 111, 201
Tafalla, M., Bachiller, R., & Martín-Pintado, J. 1993, ApJ, in press
Ungerechts, H., & Thaddeus, P. 1987, ApJS, 63, 645
Wouterloot, J. G. A., Walmsley, C. M., & Henkel, C. 1988, A&A, 191, 323 (WWH)